Quadruplex-Coupled Kinetics Distinguishes Ligand Binding between G4 DNA Motifs†

Kangkan Halder and Shantanu Chowdhury*

Proteomics and Structural Biology Unit, Institute of Genomics and Integrative Biology, CSIR, Mall Road, Delhi 110 007, India

Received August 8, 2007; Revised Manuscript Received October 9, 2007

ABSTRACT: G-quadruplex (or G4 DNA) specific ligands are important potential anticancer molecules as telomerase inhibitors. On the other hand, emerging evidence implicates G4 DNA in regulation of several oncogenes making telomerase inhibitors amenable to undesired effects (Borman, S. (2007) *Chem. Eng. News 85* (22), 12−17). Therefore molecules which can discriminate between G4 DNA are of interest, both as telomerase inhibitors and for selective intervention of gene expression. Design of selective molecules requires resolution of the coupled equilibria between intramolecular quadruplex-formation and bimolecular ligand-binding. Several previous studies have reported G4−ligand binding kinetics, however the primary equilibrium of intramolecular G4 DNA folding/unfolding was not considered. Here, we quantitatively assess the linked equilibrium in G4−ligand complexes using a novel real time surface plasmon resonance-based technique. Kinetic constants for G4 folding/unfolding and ligand binding were simultaneously determined, for the first time, from a single reaction by resolving the coupled equilibrium. We demonstrate the coupled model by showing that affinity of TMPyP4 (a well-established anticancer telomerase inhibitor) for the human telomere quadruplex is only 3-fold more than the *c-MYC* promoter G4, which is known to repress *c-MYC*. This provides quantitative rationale to poor selectivity of TMPyP4 in recently observed cell-based assays. In the light of recent advances indicating G4's regulatory potential in several important genes, quantitative evaluation of selectivity vis-à-vis affinity as presented here will augment design and preliminary screening of new molecules.

Several G-quadruplex (or G4 DNA) specific small molecule ligands (derivatives of porphyrins, perylenes, amidoanthraquinones, amidofluorenones, acridines, triazines, fluoroquinoanthroxazines, indoloquinolines, dibenzophenanthrolines, (reviewed in (*1*−*3*)) and recently telomestatin and selenium-substituted porphyrin (*4*) are of interest as anticancer drugs for telomerase inhibition resulting from binding to G4 motifs within human telomeres. On the other hand, emerging evidence shows that promoters of important genes like β-globin (*5*), retinoblastoma susceptibility (*6*), insulin (*7*), PDGF (*8*), *c-kit (9*) and *c-MYC* (*10*, *11*) also harbor putative G4 motifs (reviewed in (*12*)). This poses a potential cross-reactivity problem for G4-based telomerase inhibitors. Indeed, recent results indicate that TMPyP4,[1] a well-established anticancer telomerase inhibitor, represses the *c-MYC* expression by binding to a promoter G4 motif (*10*). Thus design of ligands exploiting G4 DNA specific structural features is necessary to achieve selectivity (*4*). Though several studies have focused on ligand binding to G4 motifs, none of these have addressed the effect of the dynamic intramolecular folding/unfolding kinetics of the motif itself, which can potentially facilitate/hinder the ligand interaction (due to half-life of the folded conformation) and also represents the dynamic intracellular conditions.

Sequence versus structural specificity of nucleic acid−drug interactions have been addressed by several methods including competition dialysis (*13*) and more recently by a modified thermal denaturation method (*14*). Here we show a quadruplex-coupled ligand association model (Figure 1a) where the kinetic rates of unimolecular folding/unfolding of the G4 in the presence of the ligand and bimolecular ligand binding to the folded G4 can be resolved concurrently from the same reaction. We demonstrate our approach using G4 motifs from the *c-MYC* promoter and human, *Oxytricha* and *Tetrahymena* telomeres and TMPyP4 and its analogue TpPy (Figure 1b). TMPyP4 was chosen to quantitatively gauge its selective potential - telomeric versus *c-MYC* promoter G4 binding. Our results, for the first time, address this issue in a quantitative kinetic evaluation. We observed that although TMPyP4 has >10-fold higher kinetic affinity for the human telomeric G4 relative to the *c-MYC* quadruplex, its equilibrium binding affinity for the telomeric motif is only 3-fold more, supporting and rationalizing recently observed marginal selectivity in cell-based competition assays (*15*, *16*). We also measured the potential of G4 motifs toward duplex formation in the presence of ligand. This revealed that at ligand/complementary strand ratios exceeding 10^2, ligand-bound G4 will result in most cases. TpPy stabilized all G4 motifs to a greater extent relative to TMPyP4 but lacked selectivity toward any particular motif. The label-free

† This research was supported by a fellowship to K.H. (CSIR) and grants to S.C. from DST, India (Fast Track Programme).

* To whom correspondence should be addressed. Fax: (91) 11 2766 7471. Phone: (91) 11 2766 6156. E-mail: shantanuc@igib.res.in.

[1] Abbreviations: SPR, surface plasmon resonance; TMPyP4, 5,10,-15,20-tetrakis(*N*-methyl-4-pyridyl)-21,23*H*-porphyrin tetrachloride; TpPy, 5,10,15,20-tetrakis(α-pyridinio-*p*-methylphenyl)-21,23*H*-porphyrin tetrachloride; QC, quadruplex-coupled; QCL, quadruplex-coupled ligand; NHE, nuclease hypersensitive element.

10.1021/bi701590z CCC: $37.00
Published on Web 12/04/2007

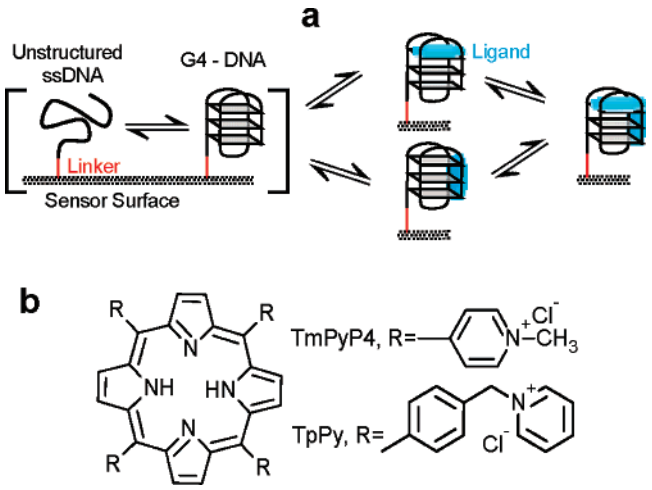

FIGURE 1: Schematic for (a) the quadruplex coupled ligand binding model and (b) porphyrin ligands used, TMPyP4 and TpPy.

technology and other advantages of SPR (*17*−*19*) makes this a viable approach for screening potential drug candidates against newly identified G4 regulatory motifs vis-à-vis their telomere binding affinity.

Kinetic Analysis: G4-Coupled Ligand Association Using SPR. The method is based on surface plasmon resonance (SPR) applied to an optical biosensor (from BIAcore Inc.), that enables real time detection of molecular association and dissociation by monitoring change in refractive index due to alteration in mass on the optical sensor (*20*). The basic method and the theoretical background have been described in detail previously (*21*−*23*).

Herein we propose a quadruplex-coupled-ligand (QCL) binding model, which simultaneously determines rate constants for small molecule (ligand) binding and folding/unfolding dynamics of the G4 (surface immobilized). Equations used in the kinetic analysis are summarized here (for details of mathematical derivation see Supporting Information). The pre-equilibrium (before ligand injection) is defined as the structural interconversion between two possible conformations of the oligonucleotide on the sensor surface. So, the surface pre-equilibrium could be expressed as

$$F \underset{k_f}{\overset{k_u}{\rightleftharpoons}} U \tag{1}$$

where k_u and k_f are the unfolding and folding rate constants of the folded conformation F and the unfolded isoform U, respectively. Here we considered that the ligand interacts with only the folded form (G4), F, in two mutually independent reactions, which may be represented as

$$F_e + P \underset{k_{d1}}{\overset{k_{a1}}{\rightleftharpoons}} C_1 \tag{2}$$

$$F_e + P \underset{k_{d2}}{\overset{k_{a2}}{\rightleftharpoons}} C_2 \tag{3}$$

where F_e is the amount of pre-equilibrated folded species present on the sensor surface, P is the ligand (porphyrin) concentration, C_1 and C_2 are G4−ligand complexes (due to P binding to two distinct binding sites) with k_{a1}, k_{d1} and k_{a2}, k_{d2} as respective association and dissociation rate constants. The rate law expression for the above set of interactions can be summarized as

$$C_1 = \left\{\frac{Pk_{a1}k_fR_{max}(1 - e^{-((Pk_{a1}+k_{d1})(t-t_0))})}{((Pk_{a1} + k_{d1})(k_u + k_f))}\right\} \tag{4}$$

$$C_2 = \left\{\frac{Pk_{a2}k_fR_{max}(1 - e^{-((Pk_{a2}+k_{d2})(t-t_0))})}{((Pk_{a2} + k_{d2})(k_u + k_f))}\right\} \tag{5}$$

where R_{max} is the is the amount of oligonucleotide immobilized on the sensor surface, t is the time elapsed after ligand injection and t_0 is the injection start time. In principle, ligand interaction with pre-equilibrated folded molecules (F_e) disturbs the pre-equilibrium. As a result, in the presence of ligand (during injection) pre-equilibrated unfolded isoforms (U_e) present on the sensor surface would give additional folded molecules (F_t) according to

$$U_e \underset{k_u}{\overset{k_f}{\rightleftharpoons}} F_t \tag{6}$$

and potentially result in additional ligand−G4 complexes. Since the folding rate is very slow compared to the rates of association of both the modes of complex formation, the above kinetic expression becomes the rate determining step and hence the overall expression would be

$$C_t = \left\{\frac{k_uR_{max}(1 - e^{-k_f(t-t0)})}{(k_u + k_f)}\right\} \tag{7}$$

where C_t is the complex formed due to the interaction of ligand and the folded species generated during the injection. Finally, the real-time response (RU) observed due to the QCL sensorgram can be mathematically expressed as the summation of all the above components for the association phase ($R_{t(assoc)}$) as

$$R_{t(assoc)} = C_1 + C_2 + C_t + R_i = \left\{\frac{Pk_{a1}k_fR_{max}(1 - e^{-((Pk_{a1}+k_{d1})(t-t_0))})}{((Pk_{a1} + k_{d1})(k_u + k_f))}\right\} + \left\{\frac{Pk_{a2}k_fR_{max}(1 - e^{-((Pk_{a2}+k_{d2})(t-t_0))})}{((Pk_{a2} + k_{d2})(k_u + k_f))}\right\} + \left\{\frac{k_uR_{max}(1 - e^{-k_f(t-t_0)})}{(k_u + k_f)}\right\} + R_i \tag{8}$$

where R_i is a fitting parameter which accounts for any response change due to the alteration in bulk refractive index between running buffer and ligand injection buffer and has been discussed previously (*21*).

Dissociation of the G4−ligand complex is given by the sensorgram after the ligand injection is stopped. A biphasic dissociation due to two binding components may be expressed as (*21*)

$$R_{t(diss)} = R_{amp1}(1 - e^{-k_{d1}(t-t_i)}) + R_{amp2}(1 - e^{-k_{d2}(t-t_i)}) + R_{(t\to\infty)} \tag{9}$$

where $R_{t(diss)}$ is the actual signal observed during dissociation expressed in response units (RU) at any time t after the ligand injection stop time t_i, R_{amp1} and R_{amp2} are defined as the amplitudes of the dissociation curve due to two binding

Table 1: Oligonucleotides (5′-3′) Used in This Study[a]

mycG17B	biotin-(act)$_3$GGGTGGGGAGGGTGGGG
mycG27B	biotin-(act)$_3$TGGGGAGGGTGGGGAGGGTGGGG-AAGG
mycG31B	biotin-(act)$_3$GGGGAGGGTGGGGAGGGTGGGGAA-GGTGGGG
htG21B	biotin-(act)$_3$GGGTTAGGGTTAGGGTTAGGG
ttG22B	biotin-(act)$_3$GGGGTTGGGGTTGGGGTTGGGG
ofG28B	biotin-(act)$_3$GGGGTTTTGGGGTTTTGGGGTTTT-GGGG
FmycG27T	**F**-TGGGGAGGGTGGGGAGGGTGGGGAAGG-**T**
FhtG21T	**F**-GGGTTAGGGTTAGGGTTAGGG-**T**
FofG28T	**F**-GGGGTTTTGGGGTTTTGGGGTTTTGGGG-**T**
FttG22T	**F**-GGGGTTGGGGTTGGGGTTGGGG-**T**

[a] mycG31, mycG27 and mycG17 are 31, 27 and 17 -mer oligonucleotide from the same nuclease hypersensitive element (NHE III$_1$) in the *c-MYC* promoter upstream of the P1 transcription initiation site; htG21, ttG22 and ofG28 are 21-, 22- and 28-mer sequences from the human, *Tetrahymena* and *Oxytricha* telomeres, respectively. Suffix B indicates 5′-biotinylated oligonucleotides, wherein 9-mer spacers (shown in lower case) at the 5′-end was used for immobilization on the sensor surface. 5′-Fluorescein (**F**) and 3′-TAMRA (**T**) end-labeled oligonucleotides were used for FRET experiments.

modes and $R_{(t\rightarrow\infty)}$ is the response value after infinite time and represents complete dissociation of the complex.

EXPERIMENTAL PROCEDURES

All oligodeoxynucleotides (Table 1) were obtained in HPLC purified state from Sigma Genosys. TMPyP4 and TpPy were purchased from Porphyrin Systems GbR, Germany. Single strand concentrations of oligonucleotides were determined using molar extinction coefficient calculated according to Gray (*24*).

Surface Plasmon Resonance. SPR measurements were performed with the BIAcore 2000 system (BIAcore Inc.) using streptavidin-coated sensor chips (Sensor chip SA, BIAcore Inc.) essentially as described before (*25*). The 5′-biotinylated sequences, each having a 9-mer spacer, were immobilized on flow cells. Flow cell 1 was kept blank (control) to account for any signal generated due to bulk solvent or any other effect not specific to the interaction, which was subtracted from the signal obtained in the oligonucleotide immobilized flow-cell. All experiments were performed at 25 °C using running buffer (0.22 μm filtered and degassed 10 mM HEPES, 150 mM KCl, 0.005% surfactant IGEPAL) at pH 7.4. Small molecule binding reactions were performed with TMPyP4 or TpPy (5−80 μM). Ligand solutions prepared in running buffer were injected (at 20 μL/min for 180 s) in random series to avoid any systematic error, using automated protocol and dissociation from the surface was monitored for next 300 s in running buffer. Regeneration was done using 1 M KCl in 50 mM KOH, as the running buffer could not completely dissociate the complex from the surface, followed by a stabilization period of 15 min in running buffer to establish pre-equilibrium on the sensor surface. Mass transfer analysis done at varying flow rates (5, 20, 50 μL/min) showed no significant difference in association rates. Sensorgrams were obtained for duplicate injections before fitting to respective equations to extract kinetic parameters. The BIAevaluation 3.1.1 software supplied by manufacturer was used to compile the QCL binding model. Alternative fitting models to test the interaction representing 1:1 Langmuir binding, heterogeneous ligand parallel/sequential binding or two state reaction with conformational change were also used, as provided by the manufacturer (BIAevaluation 3.1.1). The dissociation phase was used to determine k_{d1} and k_{d2}, which were then used in the association phase to extract k_f, k_u, k_{a1} and k_{a2}.

Fluorescence Resonance Energy Transfer (FRET). Scans were recorded on Fluoromax 3 (SPEX) spectrofluorimeter with an excitation and emission bandwidth of 5 and 5 nm respectively, and a 3 mL 1 × 1 cm quartz cuvette. TMPyP4 or TpPy (0.05−10 μM) was added to 100 nM of doubly labeled oligonucleotides (Table 1) in 10 mM HEPES, 100 mM KCl, pH 7.4 at 25 °C. Excitation wavelength was set to 480 nm (though the absorption maxima of donor, fluorescein, is at 492 nm) to minimize acceptor absorption. Emission spectra were recorded from 500 to 750 nm after equilibrating for 30 min.

Circular Dichroism (CD). Measurements were performed on a Jasco spectropolarimeter (model J 715) equipped with a thermostat controlled cell holder with a cell path length of 1 cm as described previously (*25*). Samples were equilibrated for at least 2 h before addition of TMPyP4 or TpPy (60 μM) before recording CD spectra from 230 to 330 nm with an averaging time of 3 s.

RESULTS

Quadruplex-Coupled Model for Ligand Binding. Continuous flow of buffer on the sensor chip following completion of ligand injection limits reversible ligand−sensor association. This in effect simplifies application of kinetic rate equations on the dissociation phase of the reaction (*21*). Hence it is general practice in SPR to fit the dissociation reaction first. We observed a clear biphasic dissociation mode (Figure 2a−d). Figure 2e shows that a monophasic dissociation fitting, as illustrated by a single ligand-binding 1:1 langmuir model, was not satisfactory. Therefore a biphasic dissociation model was necessary, whereby a two-site binding model was considered. We first tested simple models like two-site heterogeneous ligand (parallel) binding (Figure 2f) and two-state conformational change (sequential) reaction (Figure 2g), but large deviations in rate constants were observed in both cases. This indicated the presence of additional interactions, which were not being adequately represented in the simple two-site models. Considering the presence of a surface equilibrium we developed the QCL binding model (see above) and observed significantly improved results with fitting-errors almost always within 5% (Figure 2a−d and Table 2). Furthermore, the QCL model addressed two key issues: first, the critical issue with respect to the folded structure, i.e., inherent folding/unfolding kinetics of the G4 motif whereby ligand association with the folded motif would be competed by inherent unfolding propensity of the structure (Figure 1a); second, ligand binding to both pre-equilibrated folded G4 on the sensor surface (F_e) and real-time G4 molecules folding during ligand injection (F_t) was considered. Sensorgram fitted to QCL model without considering the F_t component resulted in high fitting-errors, (Figure 2h), supporting the necessity of the sensor surface equilibria.

Keeping in mind the possible artifacts in SPR experiments, we confirmed the biphasic binding observed in SPR by

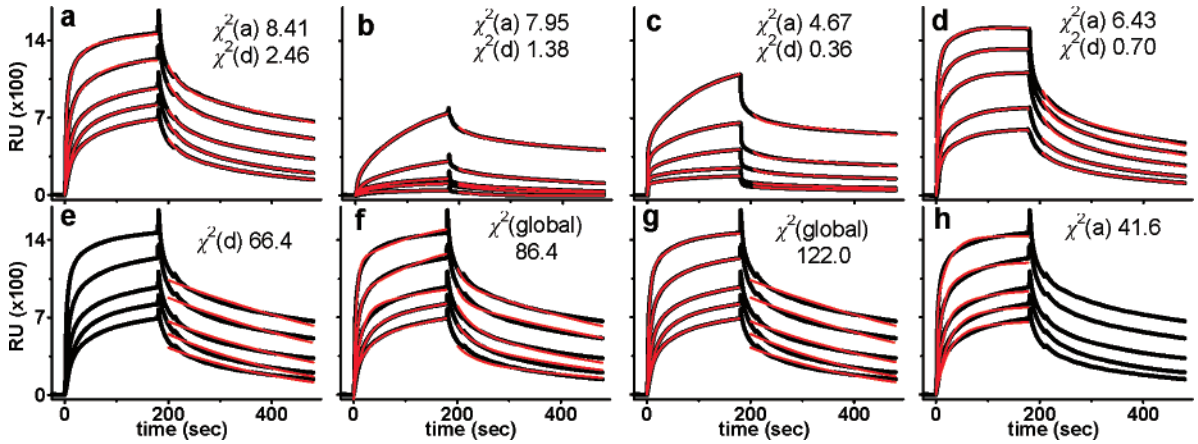

FIGURE 2: Sensorgrams were obtained by ligand binding to immobilized biotinylated G4 DNA sequences (Table 1) using 5, 10, 20, 40 or 80 μM ligand in the mobile phase. Fitted curves (red) were obtained by fitting the sensorgrams (black) for immobilized mycG27B (a, b) or htG21B (c, d) using either TpPy (a, d) or TMPyP4 (b, c) using the QCL model. Minimal requirement of QCL model was tested for mycG27B-TpPy by single dissociation mode (e); alternate global fitting models, like heterogeneous ligand binding (f) or two state conformational change binding (g) were used and (h) was equivalent to (a) except no "pre-equilibrium" component (C_t arising due to F_t) was considered. χ^2 values representing the corresponding "goodness of fit" for the association phase (χ^2(a)) and dissociation (χ^2(d)) are shown.

Table 2: Kinetic Parameters for Quadruplex Folding/Unfolding and Ligand-Binding Obtained Using the Quadruplex-Coupled Ligand Binding Model Using SPR[a]

G4−ligand		folding−unfolding				binding mode 1			binding mode 2		
		k_u (10^{-3} s^{-1})	k_f (10^{-3} s^{-1})	$t_{F_{1/2}}$ (s)	K_F	k_{a1} (10^3 M^{-1} s^{-1})	k_{d1} (10^{-4} s^{-1})	K_{D1} (10^{-8} M)	k_{a2} (10^2 M^{-1} s^{-1})	k_{d2} (10^{-3} s^{-1})	K_{D2} (10^{-6} M)
myc-G27B	P4	1.88	9.27	369	4.93	3.67	1.12	3.05	7.47	8.65	11.6
		(1.95%)	(3.33%)			(8.56%)	(0.86%)		(3.22%)	(1.02%)	
	Py	0.60	7.38	1155	12.3	8.45	2.46	2.91	13.7	8.70	6.35
		(0.78%)	(2.55%)			(3.22%)	(1.12%)		(1.21%)	(0.94%)	
htG-21B	P4	2.44	8.32	284	3.41	45.0	4.65	1.03	5.25	10.3	19.6
		(1.65%)	(3.26%)			(3.68%)	(0.88%)		(1.57%)	(0.65%)	
	Py	0.55	6.97	1260	12.7	11.2	3.76	3.36	8.85	9.25	10.5
		(1.32%)	(2.58%)			(4.77%)	(1.59%)		(1.64%)	(0.85%)	
ofG-28B	P4	5.60	9.48	124	1.69	43.8	5.43	1.24	3.83	13.3	34.7
		(1.45%)	(1.65%)			(5.55%)	(2.01%)		(2.46%)	(1.58%)	
	Py	3.23	16.7	215	5.17	14.2	2.03	1.43	13.5	8.93	6.61
		(1.58%)	(4.67%)			(5.12%)	(1.36%)		(3.22%)	(1.51%)	
ttG-22B	P4	3.68	6.48	188	1.76	2.67	3.68	13.8	3.69	9.27	25.1
		(0.99%)	(4.79%)			(4.52%)	(0.25%)		(2.56%)	(1.93%)	
	Py	1.24	12.0	559	9.68	3.86	9.45	24.5	1.72	10.3	59.9
		(3.65%)	(3.22%)			(3.71%)	(3.26%)		(1.27%)	(2.01%)	

[a] Sensorgrams were obtained with either P4 (TMPyP4) or Py (TpPy) in 150 mM K^+ at 25 °C as mentioned in Experimental Procedures and kinetic parameters extracted using the quadruplex-coupled ligand binding model (eqs 8 and 9). K_F is the equilibrium constant for quadruplex folding/unfolding during ligand binding and is calculated from k_f/k_u; K_{D1} and K_{D2} denote equilibrium dissociation constants of ligand bound G4 molecules and are given by respective k_d/k_a. Half-life of folded molecules is given by $t_{F_{1/2}}$ (=ln $2/k_u$). Numbers in parentheses are for standard errors observed during fitting.

equilibrium fluorescence resonance energy transfer (FRET) experiments. Purine-rich sequences doubly end labeled with FRET pairs, fluorescein and TAMRA, were used for this purpose (Table 1). FRET results complied with the SPR findings indicating at least two binding modes (Figure 3a,b and Supporting Information Table 1). Porphyrin binding to G4 motifs were further ascertained by CD (Figure 3c−h), wherein distinct change in peak ratio was observed in line with previous studies (*26*, *27*).

The association parameters for biphasic binding, k_{a1} and k_{a2}, indicate that the second site has more than 100-fold lower affinity in almost all cases (Table 2). This is consistent with previous reports wherein porphyrin binding was indicated to present at least one secondary site with lower affinity (*16*, *28*), however binding constants were not determined. A recent study observed TMPyP4 binding to the human telomeric G4 using SPR, wherein the coupled intramolecular folding equilibrium was not considered (*29*). The reported k_{on} was of the same order as observed by us (10^3 M^{-1} s^{-1}), and k_{off} was an order of magnitude different (10^{-3} s^{-1}); no standard errors were given in this study. Equilibrium and kinetic G4 binding affinities observed by us are in line with ones determined for other molecules using noncoupled binding models (Supporting Information Table 2), however substantially higher standard errors were observed in earlier cases. Also, most previously observed dissociation constants ranged from 10^{-2} to 10^{-3} s^{-1}, in contrast to the ones observed by us for (10^{-4} s^{-1} for binding mode 1). One possible reason could be the dissociation-fitting model used in our study, which gives improved fitting and was shown to be a more effective method in an extensive study earlier (*21*).

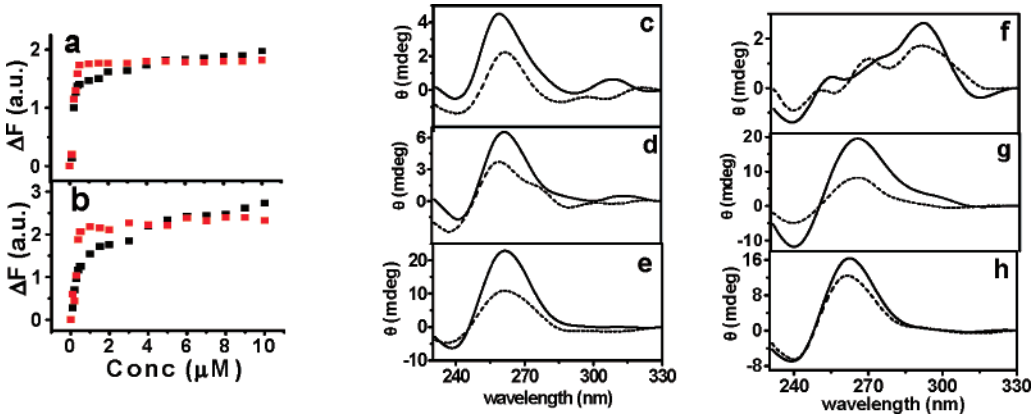

FIGURE 3: Biphasic binding was confirmed by FRET using 100 nM of FmycG27T (a) or human telomeric FhtG21T (b) titrated with TMPyP4 (black squares) or TpPy (red squares) to a final concentration of 10 μM ligand. Change in fluorescence emission of the acceptor fluorophore at 580 nm was monitored with increasing ligand concentration, 30 min after each addition. The plots were analyzed using the Scatchard protocol, and results are given in Supporting Information Table 3. CD spectra of 3 μM *c-MYC* (17-mer (c), 27-mer (d), 31-mer (e)) and telomeric (human (f), *Oxytricha* (g) and *Tetrahymena* (h)) G4 DNA in the free form (solid line) or bound to 60 μM TpPy (dashed line). Similar spectra were observed with TMPyP4 (data not shown).

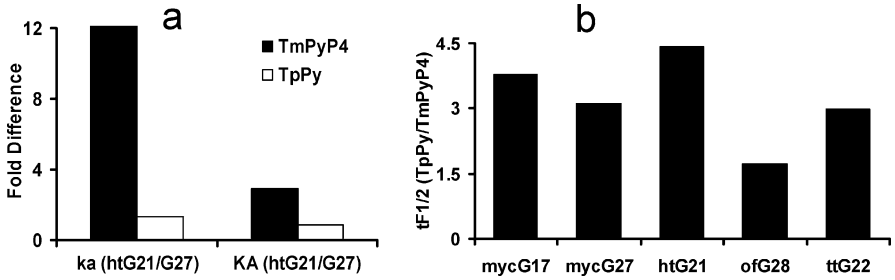

FIGURE 4: TpPy confers higher stability to G4es relative to TMPyP4 whereas TMPyP4 is more selective. (a) Comparison of kinetic (k_a) and equilibrium (K_A) affinity of respective ligands for the human telomeric (htG21B) versus the *c-MYC* (mycG27) G4 DNA. (b) Stability of the folded species in TpPy relative to TMPyP4 (expressed as a ratio of respective $t_{F_{1/2}}$) for respective G4 motifs as determined from the quadruplex-coupled ligand (QCL) binding model; values for respective $t_{F_{1/2}}$ are given in Table 2.

TMPyP4 Affinity for the Human Telomeric G4 Is Only 3-fold Higher versus the c-MYC G4. Competition experiments to evaluate selectivity of TMPyP4 for *c-MYC* with respect to telomeric G-quadruplex motifs have given contrasting results. A recent cell-based assay by Lemarteleur et al. (*15*) indicated marginal difference in selectivity while, in an another report, the affinity of TMPyP4 for the *c-MYC* quadruplex was estimated for almost ~8-fold higher (*16*) (see Supporting Information). In order to address this issue quantitatively we explored the selectivity of TMPyP4 in this respect. We observed that the kinetic affinity of TMPyP4 for the human telomeric quadruplex is ~12-fold more than the *c-MYC* G4 while TpPy has almost similar affinity toward both (Figure 4a). This results from a comparison of the k_a for ligand association of the respective ligands observed using the QCL model. Only binding mode 1, where k_a is >100-fold higher for both the *c-MYC* and human telomeric G4, was considered for this comparison. Thus, though TpPy imparts higher stability to the folded motifs, it is poor in terms of selectivity between quadruplexes. The difference in kinetic association, however, translates to ~3-fold higher equilibrium association of TMPyP4 toward the telomeric quadruplex. The difference between the kinetic and equilibrium parameters is due to faster dissociation of TMPyP4 from the telomeric G4 relative to *c-MYC* (Table 2).

Quadruplex-Coupled Hybridization of c-MYC and Telomeric G4 Motifs. The propensity of G4 DNA for duplex formation in the presence of the complementary strand is expected to result in altered G4 DNA formation/deformation rates and hence would affect ligand binding. Moreover, this would be of significance in an intracellular context. Independent estimation of motif folding/unfolding rate constants by the QCL model and a corresponding quadruplex-coupled (QC) hybridization model (*25*) should in principle enable comparative evaluation. In order to do this we used the QC hybridization model developed by us earlier. Furthermore, two key issues could also be addressed with the above comparison. First the relative stability as determined by the "half-life" of each G4−ligand (complex) pair would help in determining a better target (G4 DNA conformation) for a particular ligand (see below). Second, this comparison was used to further validate the coupled model. Since we considered ligand binding solely with folded G4 DNA in QCL model and not with the unfolded single strand, it was expected that the unfolding rate k_u would be affected during ligand binding, while it would remain relatively unchanged during hybridization with the complementary strand; the folding rates (k_f) would be largely similar in both cases. This was found consistent and supports the quadruplex-coupled ligand binding model (Supporting Information Table 3).

TpPy-Mediated Stabilization of Quadruplex DNA Is More Effective than TMPyP4. Results from quadruplex binding events using the coupled models, during both hybridization and ligand binding, allowed us to further analyze our results in several ways. First, stabilization of the G4 motifs, both *c-MYC* and human telomeric, by TMPyP4 and TpPy was readily reflected in increased half-life of the folded motif relative to the half-lives observed in hybridization experi-

Table 3: Kinetic Parameters for Quadruplex Folding/Unfolding and Hybridization Obtained Using the Quadruplex-Coupled Hybridization Model Using SPR[a]

immobilized oligonucleotide	k_u ($\times 10^{-3}$ s^{-1})	k_f ($\times 10^{-2}$ s^{-1})	$t_{F_{1/2}}$ (s)	K_F	k_a ($\times 10^5$ M^{-1} s^{-1})	k_d ($\times 10^{-4}$ s^{-1})	K_D ($\times 10^{-10}$ M)
mycG27B	8.96 (3.76%)	1.41 (4.32%)	77	1.57	1.51 (3.56%)	3.27 (1.95%)	21.7
htG21B	7.06 (2.99%)	1.63 (3.11%)	98	2.31	1.31 (2.87%)	5.98 (2.19%)	45.6
ttG22B	7.64 (3.22%)	1.08 (3.01%)	91	1.41	2.42 (2.76%)	1.85 (2.22%)	7.64
ofG28B	11.8 (3.39%)	1.25 (4.04%)	59	1.06	4.33 (2.05%)	1.80 (1.37%)	9.65
mycG17B	10.7 (5.86%)	1.20 (6.12%)	65	1.12	3.18 (4.85%)	9.36 (2.43%)	29.4

[a] Sensorgrams were obtained in 150 mM K^+ at 25 °C and kinetic parameters extracted using the quadruplex-coupled hybridization model (*25*). K_F is the equilibrium constant for quadruplex formation during competing hybridization calculated from k_f/k_u; K_D denotes the equilibrium dissociation constant for duplex formation, given by k_d/k_a. Numbers in parentheses are for standard errors observed during fitting.

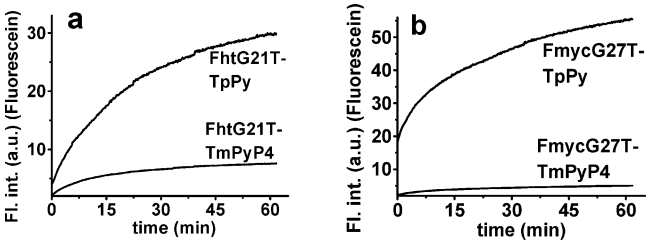

FIGURE 5: TpPy bound complexes of human telomeric and *c-MYC* G-quadruplexes were more stable than corresponding TMPyP4 complexes in a hybridization competition experiment using FRET. 50 nM of doubly labeled (5′-fluorescein and 3′-TAMRA) oligonucleotides FhtG21T (a) and FmycG27T (b) were bound to 1 μM of either TMPyP4 or TpPy followed by addition of the corresponding complementary strand (0.5 μM). Fluorescence of the donor (fluorescein at 520 nm) was monitored after excitation at 480 nm (see Experimental Procedures). All experiments were performed in 10 mM HEPES, 100 mM KCl, pH 7.4. Difference in observed amplitudes of increase in intensity of fluorescein results from unequal quenching of fluorescein emission by TMPyP4 and TpPy.

ments (Tables 2 and 3). Second, except the ofG28B quadruplex all folded motifs showed ~3−4 fold more stabilization by TpPy than TMPyP4 (Figure 4b). This was consistent with a recent observation indicating increased stabilization of the human telomeric G4 by TpPy relative to TMPyP4 (from UV-melting studies (*28*)). A similar effect on the *c-MYC* quadruplex was observed for the first time. In order to validate this observation against possible experimental artifacts in SPR we checked it by independent FRET experiments done under equilibrium conditions. Increased stabilization of human telomeric and *c-MYC* G-quadruplex by TpPy when compared to TMPyP4 (as observed by SPR) was confirmed by FRET experiments (Figure 5). Ligand-bound G4 (doubly labeled with FRET fluorophore pair) was competed with the complementary strand and the loss in energy transfer on unfolding due to hybridization observed. It was expected that increased time for hybridization would reflect the relative stability of bound molecules. An increased half-life of duplex formation with the respective complementary strand when bound to TpPy relative to TMPyP4 was found accordingly for both human telomeric (Figure 5a) and *c-MYC* G-quadruplex motif (Figure 5b), which is consistent with SPR results. Third, we analyzed quadruplex folding constants (k_f) in the presence of the complementary strand or ligand, respectively, to compare the relative stabilization conferred by ligand association. Half-life of the ligand-bound G4 versus half-life of the folded motif observed during hybridization ($t_{F_{1/2}}$(ligand)/$t_{F_{1/2}}$(hybridization)) was observed as a ratio (Figure 6a). Ligand induced stabilization of the folded motifs was clearly observed for both TMPyP4 and TpPy. Here also we observed that fold-stabilization was more in the case of TpPy than TMPyP4. Interestingly, the human *c-MYC* (mycG27) and telomeric (htG21) motifs appeared to be more stabilized than other motifs.

Hybridization versus Ligand Association Potential of Telomeric and c-MYC G4. Though the ligand-bound state resulted in higher stabilization (increased half-life with respect to the hybridized state), it was evident that all G4 motifs had higher affinity toward hybridization relative to ligand binding by more than 2 orders of magnitude. However, the ligand may easily attain ~1000-fold higher intracellular concentration than the complementary strand without being cytotoxic (*30*). We first analyzed the relative difference in kinetic and equilibrium association constants for hybridization versus ligand binding for each G4 with respect to TMPyP4 and TpPy. Interestingly, the human telomeric G4 had almost similar kinetic affinity for hybridization and TMPyP4-binding, which was due to a high k_a relative to *c-MYC* G4 (Figure 6b). This was in contrast to the case of TpPy, where the quadruplexes showed higher potential toward hybridization in both cases. However, in all cases the equilibrium association constants K_A were in favor of hybridization.

In order to judge which molecule is more suitable to win the competition between ligand-association and duplex formation, we evaluated the ligand-association potential vis-à-vis hybridization for particular ligand−G4 pairs. The ratio of ligand concentration versus complementary strand concentration was plotted against the relative rates of ligand-binding and duplex formation ($k_{obs(ligand)}/k_{obs(hybridization)}$) (see Supporting Information for details). In this case of human-telomere, htG21B−TMPyP4 pair was most effective, where more than 50-fold higher binding was achieved at about 100-fold excess of ligand (Figure 6c). Other G4−ligand pairs required an order of excess ligand to achieve the same. This is in line with the potent nature of TMPyP4 for telomerase inhibition observed by several groups in cell-based assays (*30, 31*). The contrasting nature of TpPy, which showed poor selectivity toward any G4 motif, was also indicated.

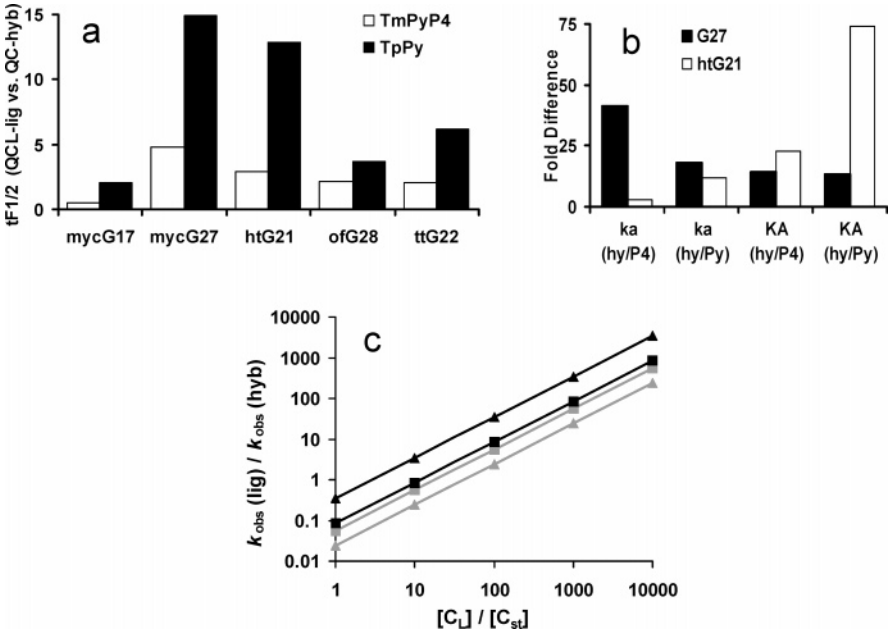

FIGURE 6: Relative stability of the folded species during ligand binding (QCL model) versus hybridization (QC model). (a) $t_{F_{1/2}}$ for hybridization was as observed from sensorgrams for hybridization (Table 3 and Supporting Information Figure 3) and $t_{F_{1/2}}$ for ligands was obtained for the respective ligands from ligand binding sensorgrams (Figure 2) and values are mentioned in Table 2. (b) Relative kinetic (k_a) and equilibrium (K_A) affinity of *c-MYC* (mycG27B) and human telomeric (htG21B) G4es for hybridization versus ligand binding. (c) Kinetic affinity of TMPyP4 relative to TpPy (ligand-association potential) versus hybridization for particular ligand−G4 pair was studied. We found that TMPyP4 binding to the human telomeric G4 in the presence of competing hybridization is found most effective relative to other ligand−G4 pairs. The ratio of ligand concentration (C_L) versus complementary strand concentration (C_{st}) was plotted against the relative rates of ligand-binding and duplex formation ($k_{obs(ligand)}/k_{obs(hybridization)}$) according to eq 20 in Supporting Information. Black triangles, htG21-TMPyP4; black squares, htG21-TpPy; gray triangles, mycG27-TMPyP4; gray squares, mycG27-TpPy.

DISCUSSION

Herein we demonstrate, for the first time, that a quadruplex-coupled ligand binding model (QCL) can be used to screen discriminatory potential of existing or newly developed G4-binding ligands against distinct structural features present within the G4 motifs. An SPR-based biphasic model was used, which considers the two competing equilibria: (a) inherent folding/unfolding of an intramolecular G4 and (b) ligand-binding to the folded G4. Concurrent resolution of (a) and (b) from a single sensorgram gives kinetic constants for both the equilibria. This is in contrast to earlier SPR studies on G4−ligand interactions (*4*, *16*, *29*, *32*, *33*). The primary difference stems from the fact that no previous study has considered the inherent folding/unfolding kinetics of the G4 forming oligonucleotide attached on the sensor surface. Therefore the effect of intramolecular folding (which depends on sequence and consequent motif architecture) on bimolecular ligand association was not addressed. Apart from this, several other differences exist. Equilibrium binding affinities for most of the ligands were in the 10^7-10^8 M^{-1} range (*4*, *16*, *29*, *32*, *33*); kinetic affinity was about 10^3 M^{-1} s^{-1}, except in the case of "3,6,9-trisubstituted acridine" binding to human telomeric G4 DNA, which showed higher affinity (Supporting Information Table 2).

Recently the first TMPyP4 bound solution structure of the 27-mer *c-MYC* G4 was solved, which clearly indicated positioning of TMPyP4 over the tetrad core instead of groove binding on the flank of the core as considered in some earlier models (*34*). However, the possibility of a second lower affinity binding inside a groove cannot be ruled out. This possibility was not addressed by the reported solution structure as the [TMPyP4]/[DNA] ratio was limited to 0.5. In these studies, a low-affinity binding mode was detected at stoichiometry greater than 1 (Phan, A. T., personal communication). Interestingly, a recent crystal structure by Parkinson et al. showed TMPyP4 in complex with human telomeric G4 DNA where two independent binding sites for TMPyP4 were clearly observed (*35*). This is consistent with our deductions suggesting two binding modes. However, the reason for different affinities of TMPyP4 for the two sites (as observed by us) is not clear from the crystal structure of the TMPyP4−G4 DNA complex. It was also noted in this study that TMPyP4 stacked over the TTA loop of the G4 motif and there was no direct interaction with the tetrad core (*35*). It is interesting to consider our results in this context. Relatively low selectivity of TMPyP4 between G4 motifs may have its molecular basis in the finding that TMPyP4 positions itself over the tetrad core without adequately engaging the core assembly. Perhaps this is the reason for somewhat similar binding affinities of TMPyP4 for human telomeric G4 DNA and duplex DNA noted in a previous SPR-based study (*29*). Based on the TMPyP4-bound structure and extensive molecular simulations with several substituted porphyrin ligands (*36*) it is tempting to speculate that the higher binding affinity of TpPy (relative to TMPyP4) may be due to the extended cationic side chains of TpPy. Using its side chains TpPy may be more favorably placed for direct interactions with the tetrad core once the ligand is lodged over the tetrad assembly helped by loop interactions as suggested by published crystal structures (*34*, *35*). Additionally, electrostatic interactions with the negatively charged phosphate residues in the backbone or exposed regions of loops may also support binding of TpPy to G4 DNA motifs.

Independent analysis of quadruplex-coupled hybridization and quadruplex-coupled ligand association allowed us to discern the respective kinetic parameters for hybridization and ligand binding. These parameters were then compared for each ligand−G4 pair (Table 2). Further, quantitative determination of individual kinetic parameters like, quadruplex folding/unfolding and ligand association/dissociation allows one to comprehend structure−activity relationships assisting rational design of substituents on particular ligands to improve/modify a desired interaction.

We have used SPR for the first time to present a quadruplex-coupled ligand association model and note that the possibility of kinetic artifacts due to one of the reactants being attached on a surface cannot be ruled out. We used a complementary equilibrium solution method, FRET, to validate our results to address the issues of kinetic artifacts and results appear to be consistent with SPR. It must also be noted that multiple folding/unfolding rates may result from the presence of more than one folded G4 motif on the sensor surface. In order to address this, we used the 17-mer *c-MYC* G4 (mycG17B), which is expected to form a single parallel motif and the observed sensorgram fittings using the QC-model are comparable. We have derived a single equation to address multiple parameters (eq 8). One of the limitations of this is that it could potentially give several minima, i.e., multiple sets of optimal values that equally fit the equation. It is difficult to completely rule out such a possibility however, typically, in such cases when optimization of all parameters is carried out simultaneously, large standard deviations result, unlike our case (errors within 5%). We further checked the effect of each parameter on the fitting by perturbing (both increase and decrease) each parameter at a time and observed its effect on the other variables. Chi-square values were observed to progressively increase indicating deviation from the correct solution in all cases (data not shown).

Several recent studies have addressed the issue of *c-MYC* G4 stabilization by telomerase inhibitors and its physiological implications (see Supporting Information (*15*, *16*, *31*)). Recent evidence indicates that several important gene promoters harbor G4 motifs (*5*−*11*, *37*), wherein the inter-relationship between the genes makes this a complex biological problem. Therefore, we understand that results of in vitro assays such as ones presented here may not directly translate into an in vivo consequence. However, selectivity vis-à-vis the target G4 may lead to decrease in cross-reactivity significantly by reducing the chances of ligand binding to multiple G4 motifs. Several studies have focused on this aspect, particularly for achieving G4 selectivity over duplex DNA binding, while recently selectivity within G4 motifs gained importance. Results presented herein demonstrate kinetic determination and use of G4 hybridization and ligand binding parameters for addressing selectivity issues, both in the context of selectivity over duplex DNA and within the G4 family. Simultaneous analysis of intramolecular G4-specific folding/unfolding rates along with bimolecular hybridization and ligand-binding parameters from linked equilibria will allow molecular fine-tuning for rational design of selective ligands. This will augment contemporary research for telomerase inhibitors, which face the new challenge of achieving selectivity over G4 regulatory elements.

ACKNOWLEDGMENT

We acknowledge Samir K. Brahmachari for constant support, Munia Ganguli for carefully reading and editing the manuscript and all members of the Chowdhury Lab for helpful discussions.

SUPPORTING INFORMATION AVAILABLE

Additional information as noted in text. This material is available free of charge via the Internet at http://pubs.acs.org.

REFERENCES

1. Neidle, S., and Read, M. A. (2000) G-quadruplexes as therapeutic targets, *Biopolymers 56*, 195−208.
2. Cuesta, J., Read, M. A., and Neidle, S. (2003) The design of G-quadruplex ligands as telomerase inhibitors, *Mini-Rev. Med. Chem. 3*, 11−21.
3. Kerwin, S. M. (2000) G-Quadruplex DNA as a target for drug design, *Curr. Pharm. Des. 6*, 441−478.
4. Rezler, E. M., Seenisamy, J., Bashyam, S., Kim, M. Y., White, E., Wilson, W. D., and Hurley, L. H. (2005) Telomestatin and diseleno sapphyrin bind selectively to two different forms of the human telomeric G-quadruplex structure, *J. Am. Chem. Soc. 127*, 9439−9447.
5. Howell, R. M., Woodford, K. J., Weitzmann, M. N., and Usdin, K. (1996) The Chicken beta-Globin Gene Promoter Forms a Novel "Cinched'' Tetrahelical Structure, *J. Biol. Chem. 271*, 5208−5214.
6. Murchie, A. I. H., and Lilley, D. M. J. (1992) Retinoblastoma susceptibility genes contain 5′ sequences with a high propensity to form guanine-tetrad structures, *Nucleic Acids Res. 20*, 49−53.
7. Catasti, P., Chen, X., Moyzis, R. K., Bradbury, E. M., and Gupta, G. (1996) Structure-function correlations of the insulin-linked polymorphic region, *J. Mol. Biol. 264*, 534−545.
8. Ma, D., Xing, Z., Liu, B., Pedigo, N. G., Zimmer, S. G., Bai, Z., Postel, E. H., and Kaetzel, D. M. (2002) NM23-H1 and NM23-H2 Repress Transcriptional Activities of Nuclease-hypersensitive Elements in the Platelet-derived Growth Factor-A Promoter, *J. Biol. Chem. 277*, 1560−1567.
9. Rankin, S., Reszka, A. P., Huppert, J., Zloh, M., Parkinson, G. N., Todd, A. K., Ladame, S., Balasubramanian, S., and Neidle, S. (2005) Putative DNA quadruplex formation within the human c-kit oncogene, *J. Am. Chem. Soc. 127*, 10584−10589.
10. Siddiqui-Jain, A., Grand, C. L., Bearss, D. J., and Hurley, L. H. (2002) Direct evidence for a G-quadruplex in a promoter region and its targeting with a small molecule to repress c-MYC transcription, *Proc. Natl. Acad. Sci. U.S.A. 99*, 11593−11598.
11. Simonsson, T., Pecinka, P., and Kubista, M. (1998) DNA tetraplex formation in the control region of c-myc, *Nucleic Acids Res. 26*, 1167−1172.
12. Shafer, R. H., and Smirnov, I. (2000) Biological aspects of DNA/RNA quadruplexes, *Biopolymers 56*, 209−227.
13. Chaires, J. B. (2005) Competition dialysis: an assay to measure the structural selectivity of drug-nucleic acid interactions, *Curr. Med. Chem.: Anti-Cancer Agents 5*, 339−352.
14. Shi, X., and Chaires, J. B. (2006) Sequence- and structural-selective nucleic acid binding revealed by the melting of mixtures, *Nucleic Acids Res. 34*, e14.
15. Lemarteleur, T., Gomez, D., Paterski, R., Mandine, E., Mailliet, P., and Riou, J. F. (2004) Stabilization of the c-myc gene promoter quadruplex by specific ligands' inhibitors of telomerase, *Biochem. Biophys. Res. Commun. 323*, 802−808.
16. Seenisamy, J., Bashyam, S., Gokhale, V., Vankayalapati, H., Sun, D., Siddiqui-Jain, A., Streiner, N., Shin-Ya, K., White, E., Wilson, W. D., and Hurley, L. H. (2005) Design and synthesis of an expanded porphyrin that has selectivity for the c-MYC G-quadruplex structure, *J. Am. Chem. Soc. 127*, 2944−2959.
17. Cooper, M. A. (2002) Optical biosensors in drug discovery, *Nat. Rev. Drug Discovery 1*, 515−528.
18. Karlsson, R. (2004) SPR for molecular interaction analysis: a review of emerging application areas, *J. Mol. Recognit. 17*, 151−161.
19. Lofas, S. (2004) Optimizing the hit-to-lead process using SPR analysis, *Assay Drug Dev. Technol. 2*, 407−415.
20. Fivash, M., Towler, E. M., and Fisher, R. J. (1998) BIAcore for macromolecular interaction, *Curr. Opin. Biotechnol. 9*, 97−101.

21. O'Shannessy, D. J., Brigham-Burke, M., Soneson, K. K., Hensley, P., and Brooks, I. (1993) Determination of rate and equilibrium binding constants for macromolecular interactions using surface plasmon resonance: use of nonlinear least squares analysis methods, *Anal. Biochem. 212*, 457−468.
22. Karlsson, R., Michaelsson, A., and Mattsson, L. (1991) Kinetic analysis of monoclonal antibody-antigen interactions with a new biosensor based analytical system, *J. Immunol. Methods 145*, 229−240.
23. Myszka, D. G. (2000) Kinetic, equilibrium, and thermodynamic analysis of macromolecular interactions with BIACORE, *Methods Enzymol. 323*, 325−340.
24. Gray, D. M., Hung, S. H., and Johnson, K. H. (1995) Absorption and circular dichroism spectroscopy of nucleic acid duplexes and triplexes, *Methods Enzymol. 246*, 19−34.
25. Halder, K., and Chowdhury, S. (2005) Kinetic resolution of bimolecular hybridization versus intramolecular folding in nucleic acids by surface plasmon resonance: application to G-quadruplex/duplex competition in human c-myc promoter 131, *Nucleic Acids Res. 33*, 4466−4474.
26. Keating, L. R., and Szalai, V. A. (2004) Parallel-stranded guanine quadruplex interactions with a copper cationic porphyrin, *Biochemistry 43*, 15891−15900.
27. Seenisamy, J., Rezler, E. M., Powell, T. J., Tye, D., Gokhale, V., Joshi, C. S., Siddiqui-Jain, A., and Hurley, L. H. (2004) The dynamic character of the G-quadruplex element in the c-MYC promoter and modification by TMPyP4, *J. Am. Chem. Soc. 126*, 8702−8709.
28. Yamashita, T., Uno, T., and Ishikawa, Y. (2005) Stabilization of guanine quadruplex DNA by the binding of porphyrins with cationic side arms, *Bioorg. Med. Chem. 13*, 2423−2430.
29. Dixon, I. M., Lopez, F., Esteve, J. P., Tejera, A. M., Blasco, M. A., Pratviel, G., and Meunier, B. (2005) Porphyrin derivatives for telomere binding and telomerase inhibition, *ChemBioChem 6*, 123−132.
30. Izbicka, E., Wheelhouse, R. T., Raymond, E., Davidson, K. K., Lawrence, R. A., Sun, D., Windle, B. E., Hurley, L. H., and Von Hoff, D. D. (1999) Effects of Cationic Porphyrins as G-Quadruplex Interactive Agents in Human Tumor Cells, *Cancer Res. 59*, 639−644.
31. Grand, C. L., Han, H., Munoz, R. M., Weitman, S., Von Hoff, D. D., Hurley, L. H., and Bearss, D. J. (2002) The Cationic Porphyrin TMPyP4 Down-Regulates c-MYC and Human Telomerase Reverse Transcriptase Expression and Inhibits Tumor Growth in Vivo, *Mol. Cancer Ther. 1*, 565−573.
32. Read, M., Harrison, R. J., Romagnoli, B., Tanious, F. A., Gowan, S. H., Reszka, A. P., Wilson, W. D., Kelland, L. R., and Neidle, S. (2001) Structure-based design of selective and potent G quadruplex-mediated telomerase inhibitors, *Proc. Natl. Acad. Sci. U.S.A. 98*, 4844−4849.
33. Teulade-Fichou, M. P., Carrasco, C., Guittat, L., Bailly, C., Alberti, P., Mergny, J. L., David, A., Lehn, J. M., and Wilson, W. D. (2003) Selective recognition of G-qQuadruplex telomeric DNA by a bis(quinacridine) macrocycle, *J. Am. Chem. Soc. 125*, 4732−4740.
34. Phan, A. T., Kuryavyi, V., Gaw, H. Y., and Patel, D. J. (2005) Small-molecule interaction with a five-guanine-tract G-quadruplex structure from the human MYC promoter, *Nat. Chem. Biol. 1*, 167−173.
35. Parkinson, G. N., Ghosh, R., and Neidle, S. (2007) Structural basis for binding of porphyrin to human telomeres, *Biochemistry 46*, 2390−2397.
36. Shi, D. F., Wheelhouse, R. T., Sun, D., and Hurley, L. H. (2001) Quadruplex-interactive agents as telomerase inhibitors: synthesis of porphyrins and structure-activity relationship for the inhibition of telomerase, *J. Med. Chem. 44*, 4509−4523.
37. Kilpatrick, M. W., Torri, A., Kang, D. S., Engler, J. A., and Wells, R. D. (1986) Unusual DNA structures in the adenovirus genome, *J. Biol. Chem. 261*, 11350−11354.

BI701590Z